Aerosol Science and Technology

ISSN: 0278-6826 (Print) 1521-7388 (Online) Journal homepage: https://www.tandfonline.com/loi/uast20

Particulate matter characteristics, dynamics, and sources in an underground mine

S. Saarikoski, K. Teinilä, H. Timonen, M. Aurela, T. Laaksovirta, F. Reyes, Y. Vásques, P. Oyola, P. Artaxo, A. S. Pennanen, S. Junttila, M. Linnainmaa, R. O. Salonen & R. Hillamo

To cite this article: S. Saarikoski, K. Teinilä, H. Timonen, M. Aurela, T. Laaksovirta, F. Reyes, Y. Vásques, P. Oyola, P. Artaxo, A. S. Pennanen, S. Junttila, M. Linnainmaa, R. O. Salonen & R. Hillamo (2018) Particulate matter characteristics, dynamics, and sources in an underground mine, Aerosol Science and Technology, 52:1, 114-122, DOI: 10.1080/02786826.2017.1384788

To link to this article: https://doi.org/10.1080/02786826.2017.1384788

AEROSOL SCIENCE AND TECHNOLOGY
2018, VOL. 52, NO. 1, 114–122
https://doi.org/10.1080/02786826.2017.1384788

Particulate matter characteristics, dynamics, and sources in an underground mine

S. Saarikoski[a], K. Teinilä[a], H. Timonen[a], M. Aurela[a], T. Laaksovirta[a], F. Reyes[b], Y. Vásques[b], P. Oyola[b], P. Artaxo[c], A. S. Pennanen[d], S. Junttila[e], M. Linnainmaa[f], R. O. Salonen[d], and R. Hillamo[a]

[a]Atmospheric Composition Research, Finnish Meteorological Institute, Helsinki, Finland; [b]Centro Mario Molina Chile, Santiago de Chile, Chile; [c]Department of Applied Physics, University of São Paulo, Rua do Matão, São Paulo, Brazil; [d]Department of Health Security, National Institute for Health and Welfare, Kuopio, Finland; [e]Outokumpu Stainless Ltd, Terästie, Tornio, Finland; [f]Work Environment, Finnish Institute of Occupational Health, Tampere, Finland

ABSTRACT

Particulate matter (PM) from mining operations, engines, and ore processing may have adverse effects on health and well-being of workers and population living nearby. In this study, the characteristics of PM in an underground chrome mine were investigated in Kemi, Northern Finland. The concentrations and chemical composition of PM in size ranges from 2.5 nm to 10 μm were explored in order to identify sources, formation mechanisms, and post-emission processes of particles in the mine air. This was done by using several online instruments with high time-resolution and offline particulate sampling followed by elemental and ionic analyses. A majority of sub-micrometer particles (<1 μm in diameter, PM_1) originated from diesel engine emissions that were responsible for a rather stable composition of PM_1 in the mine air. Another sub-micrometer particle type originated from the combustion products of explosives (*e.g.*, nitrate and ammonium). On average, PM_1 in the mine was composed of 62%, 30%, and 8% of organic matter, black carbon, and major inorganic species, respectively. Regarding the analyzed elements (*e.g.*, Al, Si, Fe, Ca), many of them peaked at >1 μm indicating mineral dust origin. The average particle number concentration in the mine was $(2.3 \pm 1.4)^{*}10^4$ #/cm^3. The maximum of particle number size distribution was between 30 and 200 nm for most of the time but there was frequently a distinct mode <30 nm. The potential origin of nano-size particles remained as challenge for future studies.

ARTICLE HISTORY
Received 12 June 2017
Accepted 16 September 2017

EDITOR
Paul Ziemann

1. Introduction

In the mine, valuable materials from ground are extracted, pre-processed, and transported for further processing. All these processes cause gas-phase and particulate matter (PM) emissions polluting air inside the mine and in the mining environment. Typically, if the ore deposits are close to the ground surface, the mine is started as open-pit and continues underground as soon as the pit is too deep for economically sound extraction without underground tunnels. Concerning the effects of mines, an open-pit mine pollutes the mine neighborhood wider than an underground mine where the dispersion of polluted air is limited. In terms of the air quality in the mine, in open-pit case the pollutants are diluted effectively by surrounding air whereas in an underground mine the efficiency of dilution depends on the mechanical and natural ventilation.

Previous studies on PM in underground mines have focused on mechanical dust which can cause high mass concentrations near the extraction and processing areas (Ghose 2007; Csavina et al. 2011; Harris et al. 2015). The effects of diesel engine emissions on the mine air quality, fine particle concentrations, and occupational exposures have also been widely investigated (Scheepers et al. 2003; Noll et al. 2007; Vermeulen et al. 2010). In a previous study conducted in an underground gold mine, it was shown that diesel exhaust can contribute by a fraction of 78%–98% to the $PM_{2.5}$ mass and by >90% to the $PM_{2.5}$ carbon concentration (McDonald et al. 2003). The role and concerns on diesel engine emissions increased when the International Agency for Research on Cancer classified diesel engine exhaust as carcinogenic to humans (WHO/IARC 2012). However, it has been suggested that the PM mass concentrations from diesel engines in

CONTACT S. Saarikoski sanna.saarikoski@fmi.fi Finnish Meteorological Institute, P.O. Box 503, FI-00101 Helsinki, Finland.
Color versions of one or more of the figures in the article can be found online at www.tandfonline.com/uast.
Supplemental data for this article can be accessed on the publisher's website.

underground mine can be reduced even by 95% when using modern exhaust after-treatment devices (Bugarski et al. 2009).

Nowadays, PM and elemental carbon (EC) concentrations in mines can be determined by real-time measurement techniques (Kimbal et al. 2012; Noll et al. 2013), but traditionally, the mass and composition of particles have been investigated by collecting particles on filters or impactor substrates, and the mass and chemical species have been determined in the laboratory (Verma et al. 1994; McDonald et al. 2002). Advanced online methods, such as aerosol mass spectrometers (AMS; Jayne et al. 2000), have originally been developed for investigation of the chemical composition of atmospheric submicrometer particles. However, they are useful also in mining environments as they can measure the composition of particles with high time-resolution from seconds to minutes allowing detection of rapidly changing situations.

In this study, physical and chemical characteristics of particulate matter were studied in a modern underground chrome mine in Northern Finland. The measurement strategy was to focus on providing high time-resolution data on concentrations and chemical composition by using stationary measurements placed 500 m below the ground level. Data allowed inspection of the diurnal cycles of pollutants and also enabled the detection of short-lasting events like blasting ore. In addition to the regular operations in the mine, the measurements were carried out during a period when fossil fuel in all diesel-engine powered vehicles working underground was replaced by renewable diesel fuel. This study focused on particles <10 μm in diameter but also particle fractions associated with occupational exposure and risk assessment (inhalable, thoracic and respirable fractions) were measured. Occupational exposure assessment is, however, out of the scope of this article. To our knowledge, this is the most comprehensive study that has investigated the chemical composition and sources of particles in an underground mine by using advanced measurement techniques such as aerosol mass spectrometry.

2. Experimental

2.1. Measurement site

The Kemi mine of Outokumpu Ltd. is the largest underground mine in Finland. It produces chromite ($FeCr_2O_4$) concentrate and raw material for the ferrochrome works in Tornio. Ore contains 25%–29% of Cr_2O_3 with a chrome to iron ratio of 1.6. The amount of sulfides in ore is very small. Annual mill capacity of Kemi mine is 2.7 million tons of ore (Source: Outokumpu Ltd.).

The air quality measurements in the mine were performed from April 24 to June 17, 2014. Measurements were carried out at a service area locating 500 m below the ground level and near the place where 190 m^3/s of supply air enters the mine via mechanical ventilation (Figure S1). The location was not in the immediate vicinity to the main drilling or ore/stone transport and handling areas that were at 425–375 m below the ground level during the measurement campaign. Thus, the measurement site represented well mixed air and was less affected by direct emissions from vehicles or operations in the mine. However, at the end of the measurement period, there were increasing activities nearby when new tunnels for future mining operations were built at 600 m below the ground level.

During this study, there were permanently 22 diesel-fuel powered vehicles in underground operations: 14 transport trucks (EURO 5 class emission control), four loaders, and four bulldozers (EURO 4 class in both types of vehicles). Normally, the diesel powered vehicles used fossil diesel fuel (EN590) but during a 6-day study period in June this fuel was replaced with 100% renewable diesel fuel (NEXBTL, hydrotreated vegetable oil, www.neste.com) in all the vehicles.

2.2. Online chemical characterization of sub-micrometer particles

The chemical characterization of PM mass below 1 μm (PM_1) was performed by using a Time-of-Flight Aerosol Chemical Speciation Monitor (ToF-ACSM, Aerodyne Research Inc., Billerica, USA, Fröhlich et al. 2013; Timonen et al. 2016). The ToF-ACSM detects non-refractory aerosol material (organic matter (OM), sulfate, nitrate, ammonium, and chloride) in sub-micrometer particles. The ToF-ACSM operated in two separate periods; first in April and second in June. Because the ToF-ACSM cannot detect sub-micrometer diesel soot (black carbon, BC), which needs higher evaporation temperature than 600°C used in the ToF-ACSM tungsten vaporizer, a Multi-Angle Absorption Photometer (MAAP, Model 5012, Thermo Scientific, Waltham, USA, Petzold and Schönlinner 2004) was used to monitor BC.

2.3. Online physical characterization of sub- and super-micrometer particles

Particle number size distributions for the sub-micrometer particles were determined by using Scanning Mobility Particle Sizers (SMPS, Wang and Flagan 1990). SMPS has a Differential Mobility Analyzer (DMA, Model 3071

Electrostatic Classifier, TSI Inc., Shoreview, USA) for particle size selection and a Condensation Particle Counter (CPC, Model 3775, TSI Inc., Shoreview, USA) to measure the particle number concentration for the selected size window. The scanned size range in this study was from 10 to 422 nm (mobility diameter, D_p). The nano-SMPS is similar to the SMPS but it uses different DMA and CPC (Model 3080 Electrostatic Classifier + Model 3085 nano-DMA+ Model 3776 CPC, TSI Inc., Shoreview, USA) enabling detection of smaller particles than with the standard SMPS. Particle size range for the nano-SMPS was 2–65 or 2–81 nm (D_p) depending on the used sheath air flow rate. Additionally, particle number concentration between 0.5 and 10 μm (aerodynamic diameter, D_a) was measured with the Aerodynamic Particle Sizer (APS, Model 3321, TSI Inc., Shoreview, USA).

The measured number concentrations of submicrometer particles (nano-SMPS, SMPS) were converted to corresponding mass concentrations by using the particle density of 1.4 g/cm^3. That average value was calculated based on the particle chemical composition measured by the ToF-ACSM and MAAP. The densities used for the chemical species were 1.2 g/cm^3 for OM (Turpin and Lim 2001), 1.77 g/cm^3 for ammonium sulfate, 1.72 g/cm^3 for ammonium nitrate, and 1.8 g/cm^3 for BC (McMeeking et al. 2010). APS number concentrations were converted to mass concentrations by using a density value of 2.0 g/cm^3 because it was assumed that super-micrometer particles contain more minerals.

2.4. Offline instrumentation

Particulate matter was collected offline by using the Nano- Micro-Orifice, Uniform-Deposit Impactor (Nano-MOUDI II, Model 125R, MSP Corp., Shoreview, USA, Marple et al. 1991, 2014) that has 13 stages between 10 nm and 10 μm (D_a). Two filter materials were used as substrates in the MOUDI; 3 μm pore size Fluoropore and 0.2 μm pore size polycarbonate membrane filters (Isopore, Merck Millipore Ltd., Billerica, USA). The total number of collected MOUDI samples was 10, of which two were analyzed for size-selective chemical composition. Additional information on the measurement devices can be found in supplementary material. The operating periods of instruments are shown in Figure S2.

2.5. Chemical analyses

The MOUDI samples were analyzed for trace elements (Na, Mg, Al, Si, S, Cl, K, Ca, Ti, Cr, Mn, Fe, Ni, Cu, Zn, Br, and P) with a high-resolution, energy dispersive X-ray fluorescence spectrometer (EDXRF, Epsilon 5, PANalytical B.V., Almelo, Netherlands) at the University of São Paulo. After the EDXRF analysis, same impactor substrates were analyzed by using ion chromatography (IC) at the Finnish Meteorological Institute. In the IC analysis, impactor substrates were extracted into 10 mL of deionised water using a short manual shaking followed by 10 min of gentle mechanical rotation. Concentrations of major inorganic anions (chloride, nitrate, and sulfate) and cations (sodium, ammonium, potassium, magnesium, and calcium) were measured simultaneously with two ICS-2000 ion chromatography systems (Dionex Corp., Sunnyvale, USA).

2.6. Data analysis

MOUDI measurements provided mass concentrations of chemical components for a total of 13 stages. The responses of the stages (collection efficiency as function of particle aerodynamic diameter) did not form a step function but instead an S-shaped curve. Therefore, inversion of the raw data using calibrated collection efficiency curves was utilized to improve the size distributions. In this work, the collection efficiency curves for the MOUDI were adopted from Marple et al. (1991). The three lowest stages of the MOUDI (cut-off diameters of 10, 18, and 32 nm) were not used in the data inversion because they had usually mass loadings close to or below detection limits of the analytical methods. The data inversion code has been developed by Wolfenberger and Seinfeld (1990) and the code for fitting of individual modes by Winklmayer et al. (1990).

3. Results and discussion

3.1. Mass concentrations and chemical composition of particles

The mass concentrations of particles with aerodynamic diameter below 0.5 μm ($PM_{0.5}$) and particles between 0.5 and 10 μm ($PM_{0.5-10}$), are shown in Figure 1 for the measurement period from April to June, 2014. The average mass concentration was larger for the fine fraction ($PM_{0.5}$) (29.9 $\pm$ 32.3 μg/m^3, average $\pm$ stdev) than for the coarse fraction ($PM_{0.5-10}$) (9.6 $\pm$ 11.2 μg/m^3). The highest hourly peaks were 100–200 μg/m^3 for $PM_{0.5}$ and 40–120 μg/m^3 for $PM_{0.5-10}$. It is obvious that the variations in the concentrations reflected varying operational activity in the mine. In general, the average mass concentrations observed in this study were much smaller than those detected earlier in a gold mine in Nevada, USA. There, the measured $PM_{2.5}$ concentrations ranged from ~400 to 2500 μg/m^3 (McDonald et al. 2002).

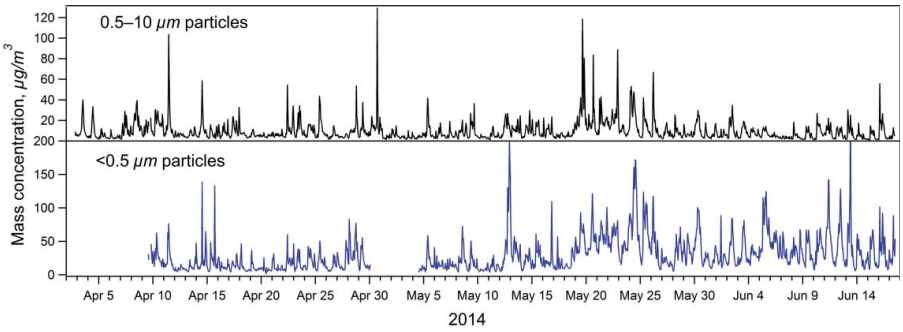

Figure 1. One hour average mass concentrations determined for coarse particles (D_a = 0.5–10 μm; APS) and for fine particles (D_a < 0.5 μm; SMPS). The APS and SMPS number concentrations were converted to mass by using particle densities of 2 and 1.4 g/cm^3, respectively.

The chemical composition of particles in sub-micrometer size range is shown in Figure 2 for the two measurement periods when the ToF-ACSM and MAAP were operating in the underground mine (April 9–18 and June 4–17, 2014). For both measurement periods, the particle mass was dominated by OM (>60% of measured species) and BC (~30%). Although the concentrations of OM and BC measured in June were almost double the concentrations measured in April, the mass fractions of OM and BC were similar during both measurement periods. OM in the mine air was a combination of hydrocarbons and oxygenated components. The average mass spectrum for OM was dominated by the fragments with mass-to-charge ratios (m/z) of 44, 28, and 18 (Figure S3a) that are mostly associated with oxygenated organic matter. However, also the pattern of hydrocarbon fragments was clear in the mass spectrum (*e.g.*, m/z 55, 57, 67, 69, and 71). The largest signal was observed for m/z 43 that typically consists of both hydrocarbon ($C_3H_7^+$) and oxygenated ($C_2H_3O^+$) fragments.

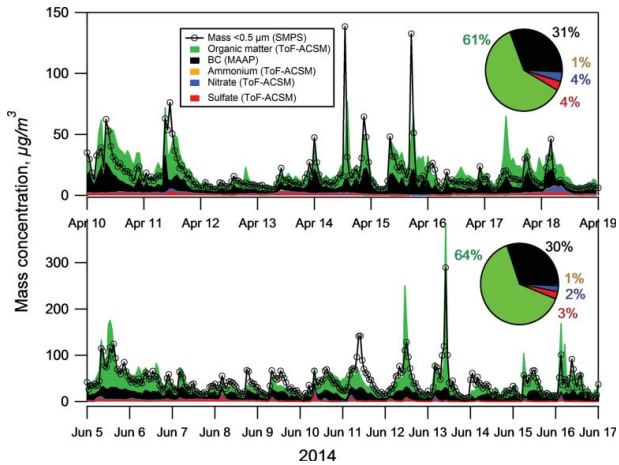

Figure 2. Chemical composition and mass closure of sub-micrometer particles in April (a) and June (b) 2014. Chemical speciation was based on the ToF-ACSM and MAAP measurements, while the total mass concentration was calculated from simultaneous SMPS data (particle density of 1.4 g/cm^3).

The oxidation state of OM was assessed by calculating the fractions of m/z 44 and 43 in the total organic signal (f_{44} and f_{43}, respectively; Ng et al. 2010). f_{44} ranged from nearly zero to 0.30 and f_{43} from 0.03 to 0.15 while the average values for the whole campaign were 0.10 and 0.084, respectively (Figure S3b). There was a difference between the April and June campaigns as f_{44} and f_{43} varied much less in June than in April. However, the average values of f_{44} and f_{43} were only slightly higher in June than in April. The average value of f_{44} corresponds to the ratio of oxygen to carbon (O:C) of ~0.5 that typically represents either low-volatility or semi-volatile oxygenated organic aerosol in the atmosphere (Ng et al. 2010).

Inorganic species constituted <10% of the total measured mass (Figure 2). The mass fractions of sulfate and nitrate were rather similar to each other (2%–4% of mass) whereas those of ammonium and chloride were much smaller (<1% of mass). Also McDonald et al. (2002) have measured the chemical composition of airborne PM in an underground mine. Like in this study, they found that most of $PM_{2.5}$ consisted of EC and organic carbon (OC) but in their data $PM_{2.5}$ was clearly dominated by EC even after converting OC to total particulate organic matter that corresponds to OM measured in this study. However, it should be noted that EC measured with thermal/optical reflectance method and BC determined optically can differ greatly due to the differences in the analytical techniques.

The sum of chemical species (ToF-ACSM+MAAP) correlated with the mass derived from the SMPS data on hourly basis (R^2 0.74 and 0.68 for April and June, respectively; Figure S4), however, the average mass from ToF-ACSM+MAAP was slightly larger than that from the SMPS. The mass concentration from ACSM+MAAP was 22.2 μg/m^3 for April and 42.4 μg/m^3 for June campaigns, on average, whereas the average mass

concentration calculated from the SMPS measurements for the April and June periods was 17.9 and 40.8 $\mu g/m^3$ (particle aerodynamic diameter <0.5 μm), respectively. The difference could be due to the assumption used in conversion from number to mass concentration by the density value (1.4 g/m^3), however, as the $PM_{0.5}$ mass was mainly composed of OM, that has typically the density in the range of 0.8–1.5 g/m^3 (Turpin and Lim 2001), that does not explain the smaller values calculated from the SMPS data. The most likely and plausible explanation is the measurement size range that has much smaller upper limit for the SMPS (0.5 μm) than for the ToF-ACSM (~800 nm) and MAAP (1 μm; Table S1).

In some cases, the mass from the SMPS was larger than that from ToF-ACSM+MAAP (Figure 2). That could be due the fact that trace elements were not included in the mass closure calculations as they could not be determined online by the ToF-ACSM or MAAP. Elements were analyzed only from two MOUDI samplings. The sum of elements (without sulfur) in the sub-micrometer particles was 3.0 and 5.1 $\mu g/m^3$ for the April and June samples, respectively. This suggests that the contribution of trace elements to the sub-micrometer particle mass could be significant, even >10% of total mass. Particle mass size-distributions of trace elements will be presented later in this article.

3.2. Sources of sub-micrometer particles

The main sources of sub-micrometer particles in the mine were identified on the basis of particle chemical composition, diurnal trends, and size distributions. In Figure S5, the diurnal variations in the concentrations of $PM_{0.5}$ and $PM_{0.5-10}$, OM and BC are shown for the April and June periods. BC, OM, and $PM_{0.5}$ followed somewhat similar trends indicating that vehicular emissions started to increase and affect $PM_{0.5}$ concentrations after ~7 AM. These concentrations stayed at their highest levels until ~2 PM, this pattern being clearest in June. In April, the level of OM was elevated between 10 AM and 3 PM.

It was obvious already from background information about the activities in the mine that there were no other major sources for OM and BC in the mine than diesel engine emissions. However, besides BC and OM, diesel engine emissions can also contribute to the measured sulfate concentration via sulfur dioxide emission and its subsequent oxidation. For sulfate, the diurnal pattern was different from BC and $PM_{0.5}$ as the largest sulfate concentrations were measured either later (in April) or earlier (in June) in the morning than the highest BC peaks. In general, there was no correlation between sulfate and BC concentrations. Actually, this could be expected because the sulfur content of modern diesel fuels is low and there were other emission sources for sulfate in the mine (*e.g.*, blasting).

Regarding emissions from blasting, there were clear 1–2 h peaks of nitrate and ammonium occurring frequently at same time (Figure S6). The most plausible explanation for those peaks is that they were residues from the ammonium nitrate and organic nitrogen based explosives used in the underground mine. At the same time with the nitrate peak, there was often a co-rise of sulfate concentration. It is possible that sulfate originated from an additive in explosives or it may have evaporated from the ore in the rock during blasting due to elevated temperature. However, ore contained low amount of sulfides. It can also be seen from Figure S6 that often before blasting, there were the smallest hourly BC and $PM_{0.5}$ mass concentrations. This is due to the fact that driving and other operations in the mine were stopped before blasting and ventilation increased. After blasting, BC and PM mass concentrations began to rise because the full-scale mining operations started again. In general, there were two major blasts in the mine on most days; at 2 PM and 10 PM. Some of the peaks observed do not coincide with these times. This is probably due to additional blasts especially in June when new tunnels were built at the level of 600 m below the ground.

In the June period, there was a 3-day experiment when fossil diesel fuel was gradually changed to 100% renewable diesel fuel (NEXBTL) in all the heavy machinery used in the underground mine. Briefly, decreased $PM_{0.5}$ and BC concentrations were not seen during the 3-day experiment with NEXBTL as could have been expected on the basis of laboratory tests comparing NEXBTL and EN590 in heavy vehicle engines (Murtonen et al. 2010). A major reason for this was probably that the trucks, having the best control of engine emissions with both fuels (EURO 5, all equipped with particle filter), had also the highest activities and largest fuel consumption during the test periods. The loaders and bulldozers (EURO 4, no particle filter) with potential to show greater decreases in particulate emissions with NEXBTL (Murtonen et al. 2010) were used much less than trucks. Thus, the overall change in particulate emissions with NEXBTL was likely small and might disappear with normal day-to-day variations in the activities. Based on fuel consumption, the mining activities were slightly smaller during the period of renewable diesel fuel (daily consumption 4200–6100 L) than in the period of fossil diesel fuel (daily consumption 4800–6900 L). Although there was no decrease in the concentration of measured air pollutants, particulate organic matter seemed to be slightly less oxidized when NEXBTL was used. f_{44} and f_{43} values were located in the same area as

the measurement data with EN590, however, f_{44} was smaller and f_{43} was larger during the NEXBTL period than on average in June (Figure S3b). In a previous study of Lutz et al. (2015), they have investigated the effect of biodiesel use on PM, OC, and EC concentrations in an underground mine. In that study, they found that 75% biodiesel/25% diesel blend was associated with reductions in respirable size PM and EC whereas respirable size OC did not change.

Besides from the sources inside the mine, some particles in the mine air are transported to the mine from outside by the ventilation. In this study, BC, OM, nitrate, and sulfate were measured simultaneously in the mine and on the ground for few days. On average, BC, OM, nitrate, and sulfate concentrations on the ground were 2.4%, 11%, 8.8%, and 45% of those in the mine, respectively. That suggests that a large fraction of sulfate was from outside air, excluding the high peaks caused by blasting (Figure S7). OM, nitrate, and especially BC had most of the sources inside the mine (diesel vehicles and blasting). BC, OM, nitrate, and sulfate were measured on the ground with a Soot Particle Aerosol Mass Spectrometer (see supplemental material).

3.3. Chemical mass size distributions

Figures S8 and S9 present particle size distributions for the elements analyzed with the EDXRF. Depending on the element, there were one or several modes peaking roughly at particle sizes 0.1, 0.5, 1, and 5 μm. The two upper modes had typically similar chemical composition, corresponding to mineral elements as shown for silicon (Figure 3) and aluminum. One possible explanation for the origins of these modes is that the largest size mode represented fresh mineral dust while the 1 μm mode was composed of aged mineral dust that had been crushed and resuspended in the air by the mining activities and ventilation. Some of the metals found in the upper modes (*e.g.*, iron and titanium) can also originate from tear and wear of mining tools and wear of diesel engines. It is likely that particles larger than 5 μm were mostly removed due to gravitational settling.

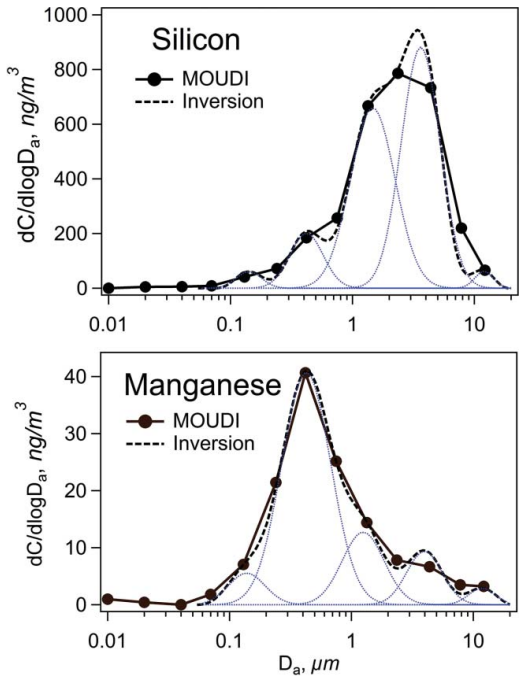

Figure 3. Mass size distributions of silicon and manganese on April 10–11, 2014. Blank values have been subtracted from the data.

The modes below 1 μm in diameter, like for manganese (Figure 3) and sulfur, could be particles from combustion of diesel fuel or lubricating oil. Phosphorus was found in sub-micrometer particles in June only. It may be a combustion product of renewable diesel fuel made of animal and vegetable material, as suggested by Zezza et al. (2012), because the MOUDI-sampling in June was performed during the NEXBTL test. However, phosphorus can also originate from lubricating oil (Pirjola et al. 2015).

In addition to the XRF analysis, the MOUDI substrates were analyzed for water-soluble inorganic ions (Figure S10). The size distributions for sulfur and sulfate analyzed with the EDXRF and IC methods, respectively, were very similar to each other. Thus, it can be concluded that most of the total sulfur consisted of water-soluble sulfate in both the April and the June samples. In April, also the size distributions for chloride, sodium, potassium, and calcium were similar with the two analytical methods. Magnesium was an exception in both April and June. With magnesium, the difference in the particle size distributions was probably due to its partial appearance in the form of talc that is water-insoluble. In June, there were generally more differences in the particle size distributions of chemical species between the two analytical methods (except for sulfur/sulfate) than in April. In June there were increased other activities than the usual operational mining of Cr-rich ore as new tunnels at 600 m below the ground level were constructed. That probably released more mineral dust to the mine air than in April. It should be noted here that the actual mass concentrations associated with elements can be higher than just the concentrations of corresponding elements because they appeared as various compounds in soil and rock. For example, stone outside of ore deposit was composed of granite and talc carbonate. Ore itself contained 25%–29% of Cr_2O_3.

3.4. Particle number size distributions

The average total number concentration of particles, as measured by the SMPS (D_p 10–422 nm), was (2.28 ±

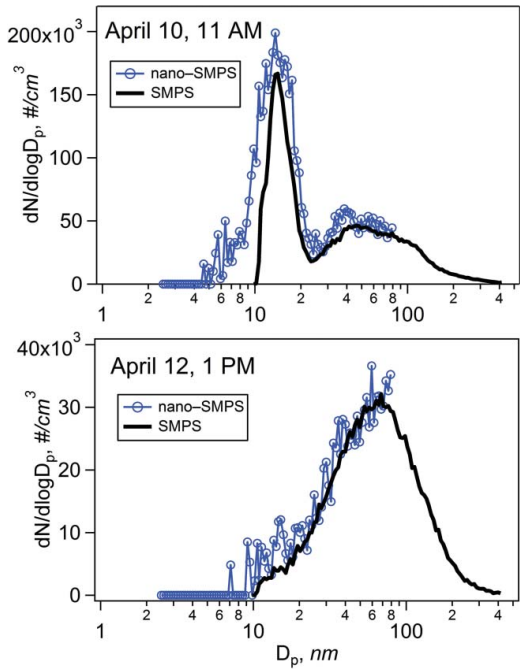

Figure 4. Size distributions measured on April 10 and April 12 (times of individual size distributions are shown by white arrows in Figure S12b).

1.40)*10^4 #/cm^3 during the measurements from April to June (Figure S11). In terms of diurnal variation, the minimum number concentration was detected between 1 and 3 AM, followed by a bi-phasic sharp rise starting around 5 AM. The maximum number concentration was achieved between 8 and 9 AM, and particle number remained elevated until 2 PM. This pattern was similar to the diurnal variation in concentrations of $PM_{0.5}$, BC, and OM, especially in June (Figure S5).

Particle number size distributions in the underground mine were either unimodal or bimodal. The peak of the particle number size distribution appeared between 30 and 200 nm for most of the time but there were regularly strong episodes when particles below 30 nm dominated the number concentration (Figure S12). The modes below 30 nm were narrow (geometric standard deviation 1.3–1.4) while the number size distribution peaking at around 0.1 μm was broader (geometric standard deviation 1.5–1.9; Figure 4). Previously, Scubacz et al. (2017) have measured particle number size distributions in a coal mine. The results obtained in this study were in line with their study since in the coal mine the total particle number concentration varied from 1.1*10^4 to 14*10^4 #/cm^3 the maximum of number size distribution being between 16 and 181 nm depending on the measurement location in the mine.

Particles below 50 nm were mostly responsible for the dynamical changes of the particle number concentration in the underground mine. In this study, it was not possible to achieve information on the composition of nanoparticles, and therefore, their origin remains unclear. One explanation is that nanoparticles are initially formed in heavy diesel vehicle engine cylinders (having size <1.5 nm), and they grow to larger size during exhaust dilution and cooling by the condensation of gaseous compounds, as suggested by Alanen et al. (2015) for natural gas engines. There were no nanoparticle events during or after blasting indicating that blasting was not the origin of these particles. New particle formation (nucleation) from gas phase precursors is another possible pathway. Because there was no daylight in the underground mine, one possible explanation for initiation of nucleation is the formation of nitrate radical (Seinfeld and Pandis 1998), a strong oxidizing agent, when ozone in ventilation air reaches NO_2 in the mine air.

4. Summary and conclusions

In this study, chemical composition, concentration, and size distribution of particulate matter were measured in an underground chrome mine in Northern Finland. When investigated in a short time-scale, the mass concentrations of $PM_{0.5}$ and $PM_{0.5–10}$ experienced fast changes, while the chemical composition of particles changed only little during the measurements. That was probably because particulate matter from diesel engine emissions, *i.e.*, OM and BC, dominated consistently $PM_{0.5}$. Blasting contributed to the mass concentrations of inorganic species (nitrate, ammonium, and sulfate) by producing high, short-lasting peaks. The origins of trace elements seemed to be either combustion (diesel engines, blasting) or mechanically formed mineral dust. Particle number size distribution measurements showed new particle formation in the underground mine. Occasionally, the newly formed nanoparticles (smaller than 30 nm) dominated the particle number concentration and were responsible for the dynamical changes in total particle number.

Regarding diesel engines, there are several ways to reduce the impacts of their emissions on the air quality in underground mines. Besides efficient ventilation, that should be mandatory in all enclosed spaces with emissions, it is important to decrease the emissions through better engine technologies, higher fuel quality, and advanced after-treatment techniques. However, it should be noted that the introduction of novel engine and exhaust after-treatment technologies into vehicles used in underground mines may change not only the quantity but also the physico-chemical characteristics and toxic properties of emissions (Murtonen et al. 2010; Jalava et al. 2012). In this study, a 3 day experiment was

conducted when fossil diesel fuel was changed to 100% renewable diesel fuel in all the vehicles in the underground mine. No changes in concentrations of $PM_{0.5}$, BC, or OM were noticed due to renewable diesel fuel. This was speculated to be caused by the steady particulate emissions of trucks that had the best emissions control for both fuels (EURO 5, equipped with particle filter). Although the particulate emission from the loaders and bulldozers (EURO 4, no particle filter) had potential to decrease with NEXBTL, they were used much less than trucks.

Advantages of the deployed set-up and approaches were obvious: (i) variations in the air quality in the underground mine could be connected to rapidly changing emissions from different mining operations, (ii) chemical composition of particulate matter revealed the major sources of sub-micrometer particles in the mine, (iii) size-distribution measurements provided a good understanding of the particulate dynamics in the mine, and (iv) detailed information on the composition, size, and sources of ambient particulate matter will allow better health risk assessment and economic air quality control in the mine. One disadvantage of this study was the lack of suitable instrumentation for investigation of the chemistry of nanoparticles. Therefore, the sources of nanoparticles in the mine could not be identified and remain as challenge for future studies.

Funding

The financial support of the Tekes Green Mining Programme for the project "Particles and noise in sustainable mining environment (HIME)" is gratefully acknowledged. This study was also funded by the Academy of Finland (grant no. 297804). The great help of the Kemi Mine staff during the measurement campaigns is highly appreciated.

References

Alanen, J., Saukko, E., Lehtoranta, K., Murtonen, T., Timonen, H., Hillamo, R., Karjalainen, P., Kuuluvainen, H., Harra, J., Keskinen, J., and Rönkkö, T. (2015). The Formation and Physical Properties of the Particle Emissions from a Natural Gas Engine. *Fuel*, 162:155–161.

Bugarski, A. D., Schnakenberg Jr., G. H., Hyummer, J. A., Cauda, E., Janisko, S. J., and Patts, L. D. (2009). Effect of Diesel Exhaust Aftertreatment Devices on Concentrations and Size Distributions of Aerosol in Underground Mine Air. *Environ. Sci. Technol.*, 43:6737–6743.

Csavina, J., Landázuri, A., Wonaschütz, A., Rine, K., Rheinheimer, P., Barbaris, B., Conant, W., Sáez, A. E., and Betterton, E. A. (2011). Metal and Metalloid Contaminants in Atmospheric Aerosols from Mining Operations. *Water Air Soil Pollut.*, 221:145–157.

Fröhlich, R., Cubison, M. J., Slowik, J. G., Bukowiecki, N., Prévôt, A. S. H., Baltensperger, U., Schneider, J., Kimmel, J. R., Gonin, M., Rohner, U., Worsnop, D. R., and Jayne, J. T. (2013). The ToF-ACSM: A Portable Aerosol Chemical Speciation Monitor with TOFMS Detection. *Atmos. Meas. Tech.*, 6:3225–3241.

Ghose, M. K. (2007). Generation and Quantification of Hazardous Dusts from Coal Mining in the Indian Context. *Environ. Monit. Assess.*, 130:35–45.

Harris, M. L., Alexander, D., Harteis, S. P., and Sapko, M. J. (2015). Collecting Representative Dust Samples: A Comparison of Various Sampling Methods in Underground Coal Mines. *J. Loss Prevent Proc.*, 36:197–204.

Jalava, P. I., Aakko-Saksa, P., Murtonen, P., Happo, M. S., Markkanen, A., Yli-Pirilä, P., Hakulinen, P., Hillamo, R., Mäki-Paakkanen, J., Salonen, R. O., Jokiniemi, J., and Hirvonen, M. R. (2012). Toxicological Properties of Emission Particles from Heavy Duty Engines Powered by Conventional and Bio-Based Diesel Fuels and Compressed Natural Gas. *Particle Fibre Toxicol.*, 9(37). doi:10.1186/1743-8977-9-37.

Jayne, J. T., Leard, D. C., Zhang, X., Davidovits, P., Smith, K. A., Kolb, C. E., and Worsnop, D. R. (2000). Development of an Aerosol Mass Spectrometer for Size and Composition, Analysis of Submicron Particles. *Aerosol Sci. Technol.*, 33:49–70.

Kimbal, K. C., Pahler, L., Larson, R., and VanDErslice, J. (2012). Monitoring Diesel Particulate Matter and Calculating Diesel Particulate Densities Using Grimm Model 1.109 Real-Time Aerosol Monitors in Underground Mines. *J. Occup. Environ. Hyg.*, 9:353–361.

Lutz, E. A., Reed, R. J., Lee, V. S. T., and Burgess, J. L. (2015). Occupational Exposures to Emissions from Combustion of Diesel and Alternative Fuels in Underground Mining—A Simulated Pilot Study. *J. Occup. Environ. Hyg.*, 12:18–25.

Marple, V., Olson, B., Romay, F., Hudak, G., Geerts, S. M., and Lundgren, D. (2014). Second Generation Micro Orifice Uniform Deposit Impactor, 120 MOUDI-II: Design, Evaluation, and Application to Long-Term Ambient Sampling. *Aerosol Sci. Technol.*, 48:427–433.

Marple, V. A., Rubow, K. L., and Behm, S. M. (1991). A Microorifice Uniform Deposit Impactor (MOUDI): Description, Calibration and Use. *Aerosol Sci. Technol.*, 14:434–444.

McDonald, J. D., Zielinska, B., Sagebiel, J. C., and McDaniel, M. R. (2002). Characterization of Fine Particle Material in Ambient Air and Personal Samples from an Underground Mine. *Aerosol Sci. Technol.*, 36:1033–1044.

McDonald, J. D., Zielinska, B., Sagebiel, J. C., McDaniel, M. R., and Mousset-Jones, P. (2003). Source Apportionment of Airborne Fine Particulate Matter in an Underground Mine. *J. Air Waste Manage. Assoc.*, 53:386–395.

McMeeking, G. R., Hamburger, T., Liu, D., Flynn, M., Morgan, W. T., Northway, M., Highwood, E. J., Krejci, R., Allan, J. D., Minikin, A., and Coe, H. (2010). Black carbon measurements in the boundary layer over western and northern Europe. *Atmos. Chem. Phys.*, 10:9393–9414.

Murtonen, T., Aakko-Saksa, P., Kuronen, M., Mikkonen, S., and Lehtoranta, K. (2010). Emissions with Heavy-Duty Diesel Engines and Vehicles Using FAME, HVO and GTL Fuels with and without DOC+POC Aftertreatment. *SAE Int. J. Fuels Lubricants*, 2:147–166.

Ng, N. L., Canagaratna, M. R., Zhang, Q., Jimenez, J. L., Tian, J., Ulbrich, I. M., Kroll, J. H., Docherty, K. S., Chhabra, P. S., Bahreini, R., Murphy, S. M., Seinfeld, J. H., Hildebrandt, L., Donahue, N. M., DeCarlo, P. F., Lanz, V. A., Prévôt, A.

S. H., Dinar, E., Rudich, Y., and Worsnop, D. R. (2010). Organic aerosol components observed in Northern Hemispheric datasets from Aerosol Mass Spectrometry. *Atmos. Chem. Phys.*, 10:4625–4641.

Noll, J. D., Bugarski, A. D., Patts, L. D., Mischler, S. E., and McWilliams, L. (2007). Relationship Between Elemental Carbon, Total Carbon, and Diesel Particulate Matter in Several Underground Metal/Non-metal Mines. *Environ. Sci. Technol.*, 41:710–716.

Noll, J., Janisko, S., and Mischler, S. E. (2013). Real-Time Diesel Particulate Monitor for Underground Mines. *Anal. Methods*, 5:2954–2963.

Petzold, A., and Schönlinner, M. (2004). Multi-Angle Absorption Photometry – A New Method for the Measurement of Aerosol Light Absorption and Atmospheric Black Carbon, *J. Aerosol Sci.*, 35:421–441.

Pirjola, L., Karjalainen, P., Heikkilä, J., Saari, S., Tzamkiozis, T., Ntziachristos, L., Kulmala, K., Keskinen, J., and Rönkkö, T. (2015). Effects of Fresh Lubricant Oils on Particle Emissions Emitted by a Modern Gasoline Direct Injection Passenger Car. *Environ. Sci. Technol.*, 49:3644–3652.

Scheepers, P. T. J., Micka, V., Muzyka, V., Anzion, R., Dahmann, D., Poole, J., and Bos, R. P. (2003). Exposure to Dust and Particle-associated 1-Nitropyrene of Drivers of Diesel-Powered Equipment in Underground Mining. *Ann. Occup. Hyg.*, 47:379–388.

Seinfeld, J. H., and Pandis, S. N. (1998). *Atmospheric Chemistry and Physics: From Air Pollution to Climate Change*. John Wiley & Sons, Inc., New York. pp. 253–254.

Skubacz, K., Wojtecki, L., and Urban, P. (2017). Aerosol Concentration and Particle Size Distributions in Underground Excavations of a Hard Coal Mine. *Int. J. Occup. Saf. Ergon.*, 23:318–327.

Timonen, H., Cubison, M., Aurela, M., Brus, D., Lihavainen, H., Hillamo, R., Canagaratna, M., Nekat, B., Weller, R., Worsnop, D., and Saarikoski, S. (2016). Applications and Limitations of Constrained High-Resolution Peak Fitting on Low Resolving Power Mass Spectra from the ToF-ACSM. *Atmos. Meas. Tech.*, 9:3263–3281.

Turpin, B. J., and Lim, H. J. (2001). Species Contributions to PM2.5 Mass Concentrations: Revisiting Common Assumptions for Estimating Organic Mass. *Aerosol Sci. Technol.*, 35:602–610.

Verma, D. K., Sebestyen, A., Julian, J. A., Muir, D. C. F., Shaw, D. S., and MacDougall, R. (1994). Particle-Size Distribution of an Aerosol and Its Subfractions. *Ann. Occup. Hyg.*, 38:45–48.

Vermeulen, R., Coble, J. B., Lubin, J. H., Portengen, L., Blair, A., Attfield, M. D., Silverman, D. T., and Stewart, P. A. (2010). The Diesel Exhaust in Miners Study: IV. Estimating Historical Exposures to Diesel Exhaust in Underground Non-Metal Mining Facilities. *Ann. Occup Hyg.*, 54:774–788. doi: 10.1093/annhyg/meq025

Wang, S. C., and Flagan, R. C. (1990). Scanning Electrical Mobility Spectrometer. *Aerosol Sci. Technol.*, 13:230–240.

WHO (International Agency for Research on Cancer). (2012). Press release no. 213, 12 June 2012.

Winklmayr, W., Wang, H.-C., and John, W. (1990). Adaptation of the Twomey Algorithm to the Inversion of Cascade Impactor Data. *Aerosol Sci. Technol.*, 13:322–331.

Wolfenbarger, J. K., and Seinfeld, J. H. (1990). Inversion of Aerosol Size Distribution Data. *J. Aerosol Sci.*, 21:227–224.

Zezza, T. R. C., Castilho, M. S., and Stradiotto, N. R. (2012). Determination of Phosphorus in Biodiesel Using 1:12 Phosphomolybdic Modified Electrode by Cyclic Voltammetry. *Fuel*, 95:15–18.